Asian Journal of Chemistry; Vol. 34, No. 9 (2022), 2217-2221

ASIAN JOURNAL OF CHEMISTRY

https://doi.org/10.14233/ajchem.2022.23790

Synthesis of ZnO/CuO Nanocomposite by Ultrasound Assisted Co-Precipitation Process using Rambutan Peel Extract

THU HANH PHAM THI, VIET BINH LE*, NGOC SON NGUYEN and THI HUONG NGUYEN*

Institute of Chemistry and Materials, 17 Hoang Sam, Hanoi, Vietnam

*Corresponding authors: E-mail: nguyenhuong0916@gmail.com; binhleviet83@gmail.com

Received: 18 February 2022; *Accepted*: 23 April 2022; *Published online*: 19 August 2022; AJC-20912

In this study, ZnO/CuO nanocomposites were synthesized by a ultrasound assisted co-precipitation method. Green synthesis of ZnO/CuO nanocomposite using rambutan peel extract as an efficient stabilizer agent has been investigated. Biosynthesized ZnO/CuO nanocomposites were characterized by X-ray diffraction (XRD), fourier transform infrared spectroscopy (FT-IR), field emission electron microscopy (FESEM), energy dispersive X-ray (EDX) and UV-Vis spectroscopy. The FESEM result showed the size of nanocomposite was 30-100 nm and had the band gap ennergy of 2.37 eV.

Keywords: Ultrasound, ZnO/CuO Nanocomposite, Ramubutan, nanocomposite.

INTRODUCTION

Zinc oxide (ZnO) is an n-type semiconductor with a wide band gap of 3.1-3.3 eV. For this material under room conditions, an energy of 60 meV is required to excite an electron to the conduction band [1]. Meanwhile, copper oxide is a p-type semiconductor with a narrower band gap of only 1.2 eV [2]. Thanks to their optical and electrical original properties [3,4], these metal oxides have been extensively studied for many applications, such as photocatalysts [5], gas sensors, energy storage materials [6,7], fuel cell [8], *etc*. To enhance semiconducting, zinc oxide and copper oxide were synthesized in nanoparticles and mixed in properly propotions [9]. There are several different methods for synthesizing hybrid nanocomposite materials ZnO/CuO have been published: coprecipitation [10, 11], hydrothermal [1,10,11], sol-gel [12] and spray pyrolysis method [13]. The common issues of these synthesis processes are quite complicated, using expensive equipment and pure chemicals which are not friendly to the environment.

Recently, green synthesis methods which used plant substances such as extraction of Rambutan peel [14], aloe vera [15], *etc*. has attracted the attention of scientists [16,17]. Asadi *et al*. [18] used *Mentha longifolia* leaf extract to synthesize ZnO/CuO nanoparticles. The resulting product has the spherical shape with a size of 30-80 nm and surface area of ZnO/CuO 5% (26 m^2/g), ZnO/CuO 10% (36 m^2/g). Yulizar *et al*. [19] synthesized ZnO/CuO nanoparticle using *Theobroma cacao* pods as the reactants. The obtained nanoparticles have a size of 20-50 nm and a band gap of 2.3 eV.

In present study, the ZnO/CuO nanocomposites by co-precipitation-ultrasonication method using rambutan peel extract (RPE). RPE containing alkaloids is used as a substitute for NaOH in the preparation of the metal oxide nanoparticles. The resulting ZnO/CuO nanocomposite which has a narrower band gap acts as a photocatalyst in the visible light area.

EXPERIMENTAL

Zinc nitrate hexahydrate ($Zn(NO_3)_2{\cdot}6H_2O$), copper nitrate trihydrate ($Cu(NO_3)_2{\cdot}3H_2O$) and ethanol were purchased form Merck. Rambutan (*Nephelium lappaceum* L.) peel was collected from Vietnam. Deionized water was used for the preparation of all aqueous solutions.

Preparation of extracts: Rambutan peel was washed with water, cut into small pieces and dried at 60 ºC until completely dry (or constant weight). The dried rambutan peels (30 g) were extracted with 600 mL of mixture ethanol and deionized water (1:2, v/v) for 30 min using a Soxhlet extractor. The extract was then filtered through Whatman No. 1 paper and stored at 5-8 ºC for further experiments.

Characterization: X-ray diffraction patterns were recorded on a P′Pret Pro-PANalyticalX-ray diffractometer operated at 1.8 kW (40 mA/45KV) using Cu*K*α (λ = 1.5406 Å) radiation. FT-IR spectra were recorded on a Bruker FT-IR spectrometer using KBr pellet method. The surface morphology and elements content of sample was imaged by field emission scanning electron microscopy (FESEM). FESEM-EDX was carried out using a Hitachi S-4800 microscope. UV-Vis (UH4150) was used to determine the band gap energy of ZnO/CuO nanocomposite. Nitrogen adsorption/desorption data were obtained at 77 K using Tristar 3000-Micromeritics equipment, USA. Samples were degassed at 75 ºC and 10^{-6} Torr for a minimum of 12 h prior to analysis. The specific surface area was calculated from the linear part of the BET plot according to IUPAC recommendation and the pore size was determined using the BJH (Barrett-Joyner-Halenda) model.

Preparation CuO/ZnO nanocomposites: Zinc nitrate hexahydrate and copper nitrate trihydrate was prepared in 100 mL deionized water and then 100 mL of rambutan peel extract (RPE) were slowly added dropwise into the solution under magnetic stirring at temperature room, and the solution was sonicated for 1 h in an ultrasonic bath (500 W, 20 kHz) to obtain a zinc-ellagate and copper-ellagte complex. The complex was collected by centrifugation at 7000 rpm for 20 min. The solid was washed with distilled water, dried in oven at 100 ºC for 2 h and then calcinated in muffle furnace at 450 ºC to obtain ZnO/CuO nanocomposites.

RESULTS AND DISCUSSION

The ZnO/CuO nanocomposites in different ratio of 90/10 and 80/20 w/w were synthesized using ramubutan peel extract (RPE), which contains phenolic antioxidants. A metal-ellagte complex was formed after 1 h sonication of solution containing rambutan peel extract and zinc nitrate hexahydrate and copper nitrate trihydrate. It was described due to the formation of bonding between hydroxyl groups of phenolic compounds and zinc metal as metal phenolate complex by the chelating effect in which the ester oxygen atoms and phenolic hydroxyl groups of phenolic compounds form π-track conjugation effect [14]. The decomposition of the metal-ellagate complex at 450 ºC to form ZnO/CuO nanocomposites.

XRD studies: The XRD peak position and their relative intensity in all XRD patterns were well-matched with the the standard cards of CuO (ICSD code no.: 067850) and ZnO (ICSD code no.: 065122). The characteristic peaks of hexagonal ZnO structure could be observed at 2θ values of 31.76º, 34.28º, 36.12º, 47.30º, 56.37º and 68.77º [19] (Fig. 1a). The XRD patterns of ZnO/CuO samples with different of CuO contents also shows all these characteristic peaks of both CuO and ZnO crystals. Interestingly, the XRD patterns exhibited broad diffraction peaks at 2θ values of 31.67º, 32.57º, 35.45º, 36.13º, 38.70º, 47.40º, 56.41º, 62.65º, 68.93º, 72.30º and 76.01º, corresponding with miller indices of ZnO and CuO were (100), (002), (101), (102), (110), (103), (111), (112), (201), (202), (311), (113) and (222) [9,20] (Fig. 1b-c).

FT-IR studies: Fig. 2 shows the FT-IR spectra of Rambutan peel extract, ZnO and ZnO/CuO samples. The FT-IR spectra of all samples showed adsorption peaks at around 3445-3300 cm^{-1} related to the OH groups and 3300-1630 cm^{-1} related to the OH groups of materials. The FTIR spectra of ext (1) shows some major peaks at 3440, 1569, 1320, 1037 and 822 cm^{-1}. The peak at 3440 cm^{-1} is attributed to O-H stretching of phenolic, band at 1569 cm^{-1} corresponds to the -COOH stretching of flavonoids and phenolic groups. The peak at 1320 cm^{-1} and 1037 cm^{-1} is due to the stretching of C-O bond in aromtic groups and C-N stretching of aromatic, aliphatic amines,which are main biological active compounds of RPE [19]. The absorption peak of ZnO (curve 4) and ZnO/CuO nanocomposite (curves 2 and 3) at wavenumber 456 cm^{-1} (curve 4) and 547 cm^{-1}, 571 cm^{-1} corresponds to the stretching vibration of Zn-O and Cu-O bonds [5,18]. However, the FT-IR spectrum displays a low intensity at 3440, 1320, 1037 cm^{-1}, indicating the decrease of functional group of RPE after calcinations.

Morphological studies: Fig. 3a shows that the ZnO surface material has particle sizes in the range of 30-100 nm. Nanocomposites are less uniform and have a smooth surface. The

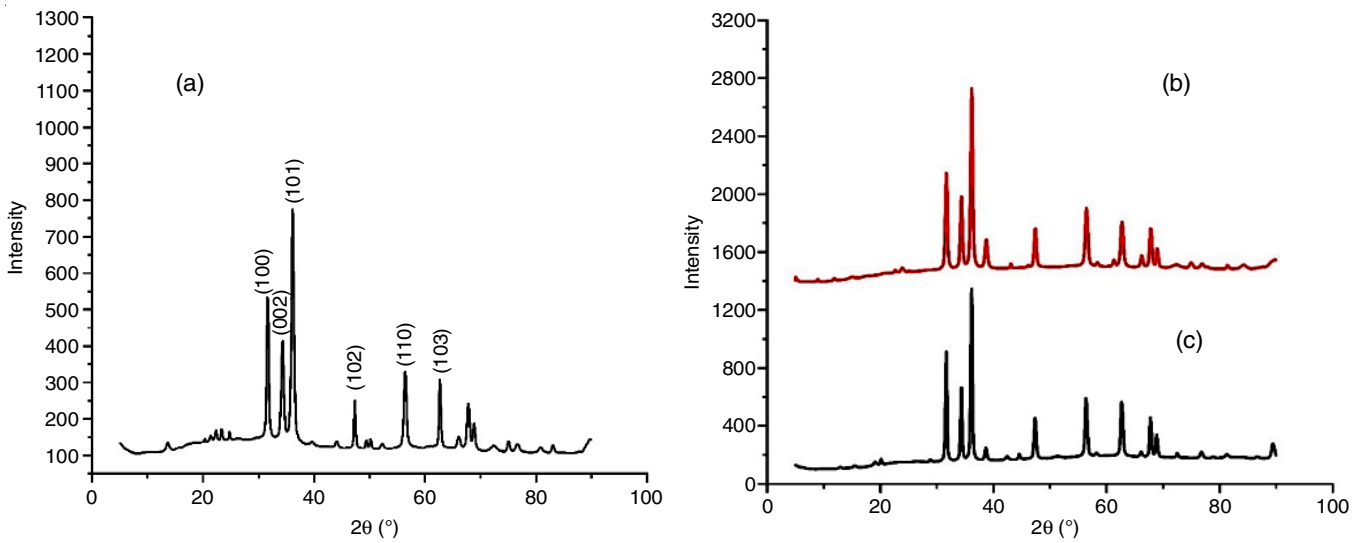

Fig. 1. XRD patterns of (a) ZnO, (b) ZnO/CuO = 90/10 w/w; (c) ZnO/CuO=80/20 w/w

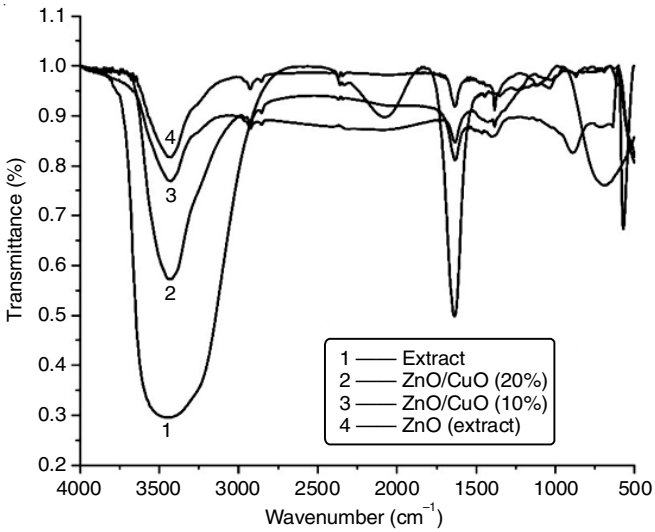

Fig. 2. FT-IR spectra of (1) ext; (2) ZnO/CuO = 80/20; (3) ZnO/CuO=90/10 w/w; (4): ZnO

images of the nanocomposite material at different magnifications show a distribution of CuO and ZnO nanoparticles with dimensions less than 100 nm. The synthetic nanocomposite therefore has a larger surface area than ZnO substrate material, which is shown using measurements of the specific surface area using the BET technique.

BET studies: The porosity characteristics of ZnO and ZnO/CuO nanocomposite were studied using BET nitrogen physisorption at -196.15 ºC. Fig. 4a-b shows the adsorption-desorption isotherm for the ZnO nanoparticles and ZnO/CuO nanocomposite. The adsorption-desorption isotherm is of type IV, as typified by the H3 hysteresis loop, rod-shaped shaped according to IUPAC classification [21]. This allows us to predict that the synthetic nanocomposite materials contain both macropores and mesopores, with large percentage of mesopores. The isotherm has two inflection points due to nitrogen uptake. The first is slow at a low relative pressure (< 0.1), and the second is sharp at a relative pressure of about 0.95, with a hysteresis loop at a relative pressure above 0.6-0.7. The higher nitrogen uptake at low relative pressure is indicative of monolayer adsorption, whereas the sharp uptake at a higher relative pressure shows multilayer adsorption. The pore size distribution is obtained from the BJH analysis. The BJH pore size distribution curve shows narrow and intense peaks. The pores size distribution curve shows that pores appear in the range 3 to 80 nm

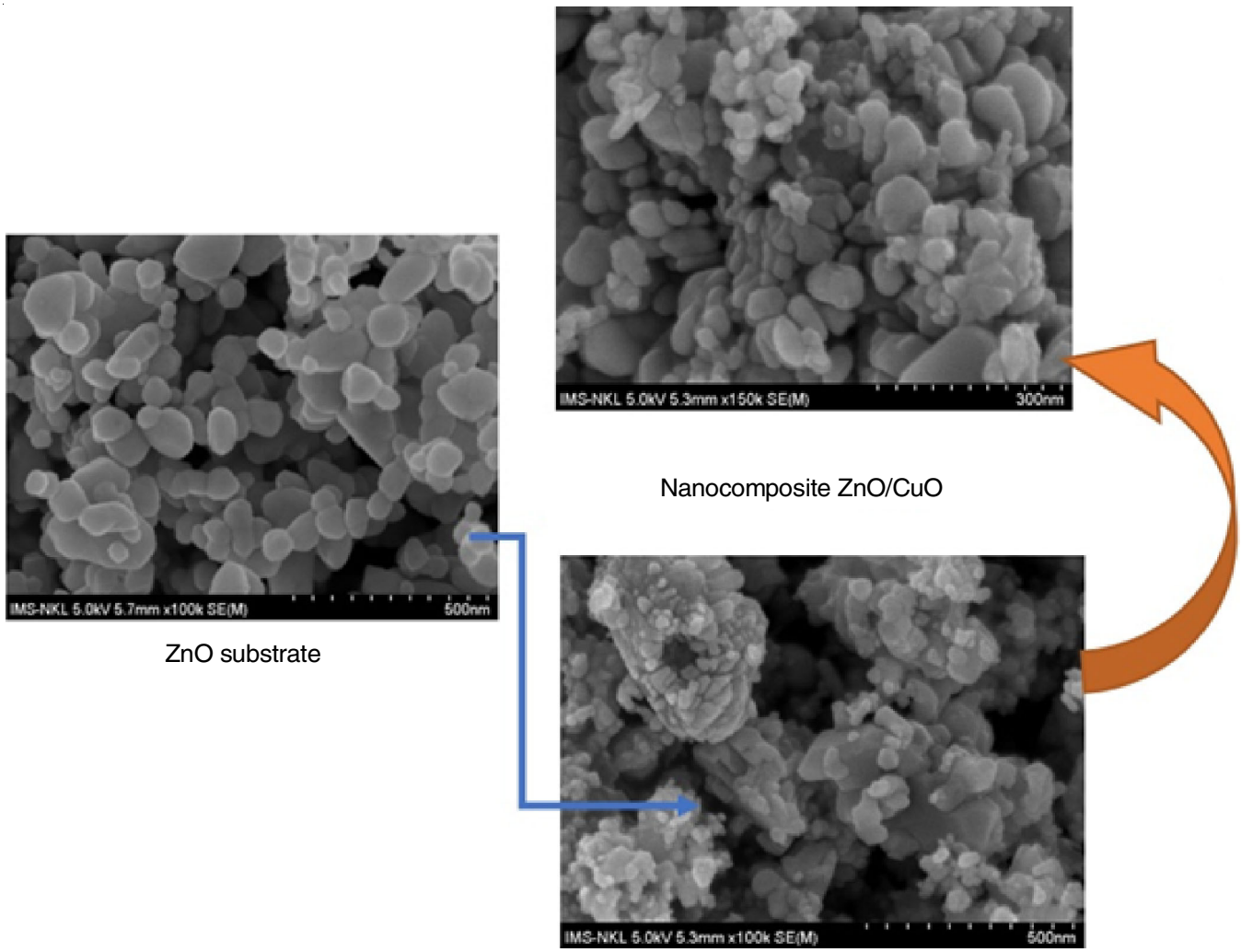

Fig. 3. FESEM images of the ZnO/CuO nanocomposite

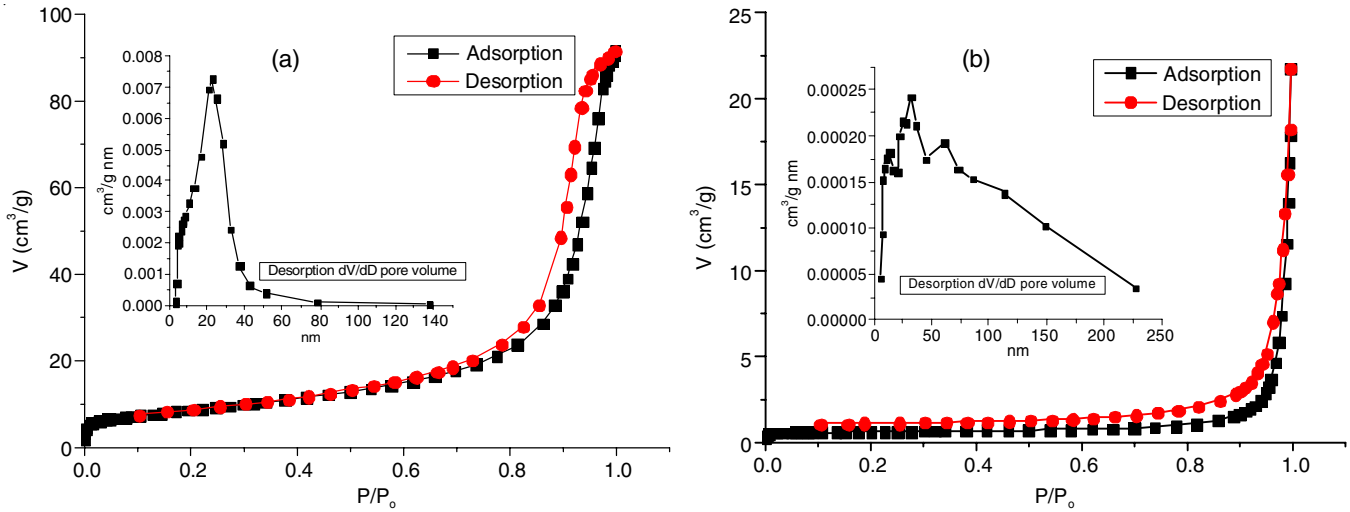

Fig. 4. Nitrogen adsorption-desorption isotherms of (a) ZnO NPs and (b) ZnO/CuO

(ZnO nanoparticles) and 3 to 200 nm (ZnO/CuO nanocomposite). The specific surface area of ZnO/CuO surface material is 25.05 $m^2 g^{-1}$, which is much smaller than that of nanocomposite material, which reaches 30.60 $m^2 g^{-1}$. The micropore area of nanocomposite $S_{micro} = S_{BET} - S_{External} = 30.60 - 19.18 = 11.42\ m^2 g^{-1}$, the pore diameter averages 19.2 nm and the total pore volume is 0.14 $cm^3 g^{-1}$.

The value of energy gap (E_g) of ZnO compound as a bulk is equal 3.31 eV but as thin film it depends on the manufacturing techniques [22,23]. The optical energy gap can be estimated by calculating the absorption coefficient (α), which depends on the film thickness (length of the absorption media) and absorbance, as given in the following equation:

$$\alpha = 2.303\left(\frac{A}{d}\right)$$

where A is the absorbance and d is the thickness. The energy gap was estimated by assuming a direct and indirect allowed transition between valence and conduction bands using the Tauc equation [22,23]:

$$\alpha h\nu = B(h\nu - E_g)^r$$

where B is constant, α is the absorption coefficient, hν is the incident photon energy, and r is constant, for direct transition r equals 1/2, and for indirect transition equals 2. Fig. 5 shows the plot of $(\alpha h\nu)^2$ *versus* hν, E_g is determined by extrapolating the straight-line portion of the spectrum to αhν = 0.

The band gap of nanocomposite E_g was determined by extrapolating the linear section of the plot to the hν axis at $(\alpha h\nu)^2 = 0$. The ZnO/CuO nanocomposite has a direct allowed energy band gap of 2.37 eV. This band gap lies between that of ZnO (3.32 eV) and CuO (1.20 eV), corresponding to elements composition from EDX results showed that ZnO/CuO nanocomposite contained were 74.90% Zn, 16.96% Cu and 8.14% O (sample 1). Therefore, by tuning the volume fractions of constituent oxides, the band gap can be engineered to make the nanocomposite suitable for several applications such as photovoltaics, solid oxide fuel cells, thermoelectrics and photocatalysis. The current study related to this work about synthesis ZnO/CuO nanocomposite by green synthesis can be seen in Table-1.

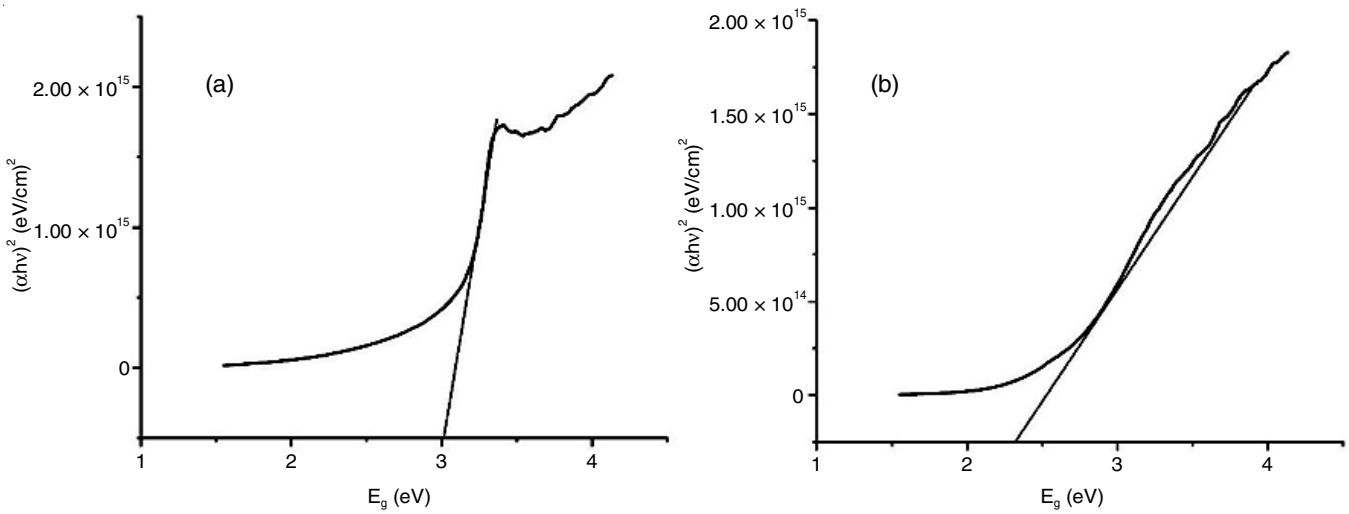

Fig. 5. Band gap of the ZnO (a) and ZnO/CuO nanocomposite (80/20) (b)

TABLE-1
COMPARISON RESULT RELATED TO SYNTHESIS OF ZnO/CuO NANOCOMPOSITE

Materials	Precursor	Stabilizing and capping agen	Methods	Particles size result	Ref.
CuO/ZnO Heterojunction	$Zn(NO_3)\cdot 6H_2O$ $Cu(NO_3)_2\cdot 3H_2O$	Propylene oxide	Micorwave -epoxide-assisted hydrothermal	34-63 nm	[24]
ZnO/CuO nanocomposite	$Zn(CH_3COO)_2\cdot 2H_2O$ $Cu(CH_3COO)_2$	350 °C/3 h in an alumina crucible	Thermal decomposition	Nanorods with an average diameter of ~35 nm and a length of 50-500 nm	[10]
ZnO NPs CuO NPs *p*-CuO/n-ZnO	$ZnCl_2$, $Cu(SO_4)_2\cdot 5H_2O$	NaOH	One-step homogeneous coprecipitation	3D microstructures-leaf-like nanopatches, diameters in the range of 1-2 µm	[9]
CuO/ZnO nanocomposite	Zn/Cu (6 mm thick Zn; Cu plates)	Succinic acid; Voltage17V	Electrochemical	90-150 nm	[24]
CuO/ZnO nanocomposite	$Zn(NO_3)\cdot 6H_2O$ $Cu(CH_3COO)_2\cdot H_2O$	*Mentha longgifolia* feaf extract	Green synthesis	30-50 nm	[18]
ZnO/CuO nanocomposite	$ZnCl_2$, $Cu(CH_3COO)_2\cdot H_2O$	KOH	Hydrothermal	ZnO: 100-300 nm;CuO: 300-500 nm	[11]
ZnO/CuO nanocomposite	$Zn(NO_3)\cdot 6H_2O$ $Cu(NO_3)_2\cdot 3H_2O$	Theobroma cacao seed brak	Green synthesis	20-50 nm	[20]
ZnO/CuO nanocomposite	$Zn(NO_3)\cdot 6H_2O$ $Cu(NO_3)_2\cdot 3H_2O$	Ramubutan peel extract (RPE)	Green synthesis (co-precipitation-ultrasonication)	30-100 nm	Present work

Conclusion

The ZnO/CuO nanocomposite materials was successfully prepared through a ultrasound assisted green synthesis using ramubutan peel extract (RPE). The FTIR characterization, flavonoids and phenolic of RPE has a role as hydrolyzing agent in ZnO/CuO nanocomposite formation. The UV-visible characterization showed that had the band gap energy of 2.37 eV, when ZnO/CuO nanocomposite contained were 74.90% Zn, 16.96% Cu and 8.14% O. The FESEM results indicated that the size of nanocomposite was 30-100 nm and the specific surface area of ZnO/CuO surface material was 30.60 $m^2\ g^{-1}$, the micropore area of pore diameter averages 19.2 nm and the total pore volume was 0.14 $cm^3\ g^{-1}$.

CONFLICT OF INTEREST

The authors declare that there is no conflict of interests regarding the publication of this article.

REFERENCES

1. Ü. Özgür, Y.I. Alivov, C. Liu, A. Teke, M.A. Reshchikov, S. Dogan, V. Avrutin, S.-J. Cho and H. Morkoç, *J. Appl. Phys.*, **98**, 041301 (2005); https://doi.org/10.1063/1.1992666
2. N.R. Dhineshbabu, V. Rajendran, N. Nithyavathy and R. Vetumperumal *Appl. Nanosci.*, **6**, 933 (2016); https://doi.org/10.1007/s13204-015-0499-2
3. M. Aminuzzaman, L.P. Ying, W.-S. Goh and A. Watanabe, *Bull. Mater. Sci.*, **41**, 50 (2018); https://doi.org/10.1007/s12034-018-1568-4
4. A. Kargar, Y. Jing, S.J. Kim, C.T. Riley, X. Pan and D. Wang, *ACS Nano*, **7**, 11112 (2013); https://doi.org/10.1021/nn404838n
5. M.A.M. Adnan, N.M. Julkapli and S.B.A. Hamid, *Rev. Inorg. Chem.*, **36**, 77 (2016); https://doi.org/10.1515/revic-2015-0015
6. A.O. Juma, E.A.A. Arbab, C.M. Muiva, L.M. Lepodise and G.T. Mola, *J. Alloys Compd.*, **723**, 866 (2017); https://doi.org/10.1016/j.jallcom.2017.06.288
7. C.-H. Lai, M.-Y. Lu and L.-J. Chen, *J. Mater. Chem.*, **22**, 19 (2012); https://doi.org/10.1039/C1JM13879K
8. E. Gopinathan, G. Viruthagiri, N. Shanmugam and S.S. Priya, *Optik*, **126**, 5830 (2015); https://doi.org/10.1016/j.ijleo.2015.09.014
9. B. Li and Y. Wang, *Superlattices Microstruct.*, **47**, 615 (2010); https://doi.org/10.1016/j.spmi.2010.02.005
10. R. Saravanan, S. Karthikeyan, V.K. Gupta, G. Sekaran, V. Narayanan and A. Stephen, *Mater. Sci. Eng. C*, **33**, 91 (2013); https://doi.org/10.1016/j.msec.2012.08.011
11. T. Chang, Z. Li, G. Yun, Y. Jia and H. Yang, *Nano-Micro Lett.*, **5**, 163 (2013); https://doi.org/10.1007/BF03353746
12. P. Jongnavakit, P. Amornpitoksuk, S. Suwanboon and N. Ndiege, *Appl. Surf. Sci.*, **258**, 8192 (2012); https://doi.org/10.1016/j.apsusc.2012.05.021
13. H.R. Ghaffarian, M. Saiedi, M.A. Sayyadnejad and A.M. Rashidi, *Iran. J. Chem. Chem.*, **30**, 1 (2011).
14. R. Yuvakkumar, J. Suresh, A.J. Nathanael, M. Sundrarajan and S.I. Hong, *Mater. Sci. Eng. C*, **41**, 17 (2014); https://doi.org/10.1016/j.msec.2014.04.025
15. K. Ali, S. Dwivedi, A. Azam, Q. Saquib, M.S. Al-Said, A.A. Alkhedhairy and J. Musarrat, *J. Colloid Interface Sci.*, **472**, 145 (2016); https://doi.org/10.1016/j.jcis.2016.03.021
16. S. Fakhari, M. Jamzad and H. Kabiri Fard, *Green Chem. Lett. Rev.*, **12**, 19 (2019); https://doi.org/10.1080/17518253.2018.1547925
17. H. Agarwal, S.V. Kumar and S. Rajeshkumar, *Resource-Efficient Technol.*, **3**, 406 (2017); https://doi.org/10.1016/j.reffit.2017.03.002
18. R. Mohammadi-Aloucheh, A. Habibi-Yangjeh, A. Bayrami, S. Latifi-Navid and A. Asadi, *J. Mater. Sci. Mater.*, **29**, 13596 (2018); https://doi.org/10.1007/s10854-018-9487-0
19. L. Sun, H. Zhang and Y. Zhuang, *J. Food Sci.*, **77**, C198 (2012); https://doi.org/10.1111/j.1750-3841.2011.02548.x
20. Y. Yulizar, R. Bakri, D.O.B. Apriandanu and T. Hidayat, *Nano-Struct. Nano-Objects*, **16**, 300 (2018); https://doi.org/10.1016/j.nanoso.2018.09.003
21. M. Thommes, K. Kaneko, A.V. Neimark, J.P. Olivier, F. Rodriguez-Reinoso, J. Rouquerol and K.S.W. Sing, *Pure Appl. Chem.*, **87**, 1051 (2015); https://doi.org/10.1515/pac-2014-1117
22. M. Alhamed and W. Abdullah, *J. Electron Devices*, **7**, 246 (2010).
23. F. Ghodsi and H. Absalan, *Acta Phys. Pol. A*, **118**, 659 (2010); https://doi.org/10.12693/APhysPolA.118.659
24. D.Y. Nadargi, M.S. Tamboli, S.S. Patil, R.B. Dateer, I.S. Mulla, H. Choi and S.S. Suryavanshi, *ACS Omega*, **5**, 8587 (2020); https://doi.org/10.1021/acsomega.9b04475